

One-dimensional transient crystalsT. Kwapiński ^{*}*Institute of Physics, M. Curie Skłodowska University, 20-031 Lublin, Poland*

(Received 23 September 2022; accepted 3 January 2023; published 20 January 2023)

A phase of solid state matter which exists in time dimension is investigated theoretically for a linear chain of quantum dots or atomic sites using the evolution operator technique and the Laplace transform technique. The studies focus on the spectral density of states (DOS) function and its modifications after a sudden quench in the system. It is shown that this function reveals a very regular structure which oscillates in time and which corresponds to the stationary DOS of one-dimensional crystals. Thus, such a system stands for a transient crystal material which exists in time dimension but appears only for a short period and suddenly vanishes. Moreover, we observe different impulse propagation velocities due to the local DOS inertia, i.e., it is more difficult to rebuild a many-peaked structure of DOS related to longer chains. We also show that the transient crystal pattern in a linear chain can be observed for real electrodes characterized by the van Hove singularities or by a flat spectral density.

DOI: [10.1103/PhysRevB.107.035422](https://doi.org/10.1103/PhysRevB.107.035422)**I. INTRODUCTION**

Recent advancements in nanotechnology enabled the investigation of low-dimensional systems such as linear quantum dots (QDs), quantum wires, or atomic chains coupled to electron reservoirs. The transport properties of such systems are of interest to scientists as they stand for the thinnest possible electric conductors [1–3] and they have many potential applications in spintronics, quantum computing, or metrology. Particularly interesting are low-dimensional conductors in the presence of time-dependent perturbations and external fields for which a wealth of effects have been predicted, such as photon-assisted tunneling [4–6], spin and charge quantum pumps [4,7–11], transient current beats [12–14], and Floquet topological insulators [15,16], to name just a few. External fields can also be used to control both the dc current and the zero-frequency noise [17,18] in mesoscopic conductors.

Recently, solid state phases which exist in the time domain were predicted in quantum systems called time crystals [19–21] and transient crystals [22]. The formation of space crystals is related to self-organization of atoms in a periodic way in space. This idea can be transformed to the time dimension so one can form spontaneously periodic structures in time in a similar way as atomic systems are arranged in space. In the most general sense time crystals are materials which somehow pulse or have structure behavior in time with their own periodicity. Such time crystal structure was proposed by F. Wilczek in 2012 [19] and then was confirmed experimentally [23,24]. These systems are able to switch to periodic motion in time under an external perturbation. The basic classification of time crystals includes both discrete [20,21] and continuous systems [25–27], depending on whether the discrete or continuous time translation symmetry is broken. For systems without any disorder terms, this symmetry can be broken by Stark many-body localization [28,29]. Also, prethermal or

metastable time crystals can exist for systems which do not relax rapidly to a ground state but undergo long-lived oscillations with complex dynamical features [30,31]. Note that discrete time crystals can be realized in periodically driven, exchange-coupled GaAs quantum dot arrays with multispin states [32]. The existence of time crystals can be manifested through the oscillations of the spin current in transport experiments and, e.g., for QD systems connected to external electrodes the oscillation amplitude decays linearly with the electrode coupling strength [33,34].

For a double site system, a sudden quench of the parameters can lead to the transient effects with evident oscillations in time of the spectral density function (also called the local density of states, DOS). This function for a given time corresponds to the electrical properties of the stationary one-dimensional (1D) crystal. Thus, it stands for a crystal that is characterized by the pulsed structure changing regularly in time with damping amplitude and is called the transient crystal [22]. However, until now there has been no research in the literature on transient crystals in other quantum systems. Transient effects in a low-dimensional system can provide insight into its electronic structure and have been intensively studied for different QD geometries [35–37]. This effect allows one to determine the parameters defining the system [36] or estimate the spin relaxation time [12]. It is worth noting that most of the transient effect studies are focused on the current or charge oscillations [35], while the quench dynamics of the spectral density function related to the quantum system has been often overlooked in the literature.

In this work, dynamical properties of one-dimensional chains are investigated, focusing on the time-dependent spectral density function and its evolution due to a sudden quantum quench. Such a system (which is the thinnest electrical conductor in space) can stand for the transient crystal material with regular oscillations of the local DOS in the time dimension. In this context it is desirable to analyze how the transient crystal structure is formed in the chain and how long it exists in time. For a double-site system the nature of the transient

^{*}tomasz.kwapinski@umcs.pl

crystal is based on the local DOS signal propagation between both sites (it balances between them in time). However, for a 1D chain this mechanism may fail due to many-coupled sites in the chain and the transient crystal may not be as evident as expected.

We are also going to determine characteristic timescales of the electrode impulse propagation through the chain just after the quench and in the transient crystal time domain. It is expected that the local DOS modifications due to the impulse propagation depend on the shape of the spectral density function, and for a rich structure of DOS (with many peaks) it takes more time to change it (there is a kind of inertia of the local DOS to change themselves in time). Thus, the signal velocity should also change during its propagation in the chain. In our studies we precisely address these problems and consider a 1D chain coupled to real electrodes characterized by different DOS functions described by the van Hove singularities or by a flat DOS. Local peaks or gaps in the electrode DOS can strongly influence the transient crystal pattern and change the impulse velocity in the system. Note that in general, using a wide-band approximation, the calculations of the electronic properties can be simplified and analytical formulas for stationary as well as for driven systems are possible [38–40]. However, beyond the wide-band limit the calculations need more sophisticated and time-consuming methods, especially in nonequilibrium phenomena [40–43]. Here, we use the evolution operator technique and the time-dependent tight-binding Hamiltonian, for which analytical calculations are possible within the Laplace transform method.

The paper is organized as follows. In Sec. II, the theoretical model with the Hamiltonian and the calculation method with an analytical solution are derived. In Sec. III, the main results of the paper are discussed for the transient crystal. In Sec. IV the role of the real DOS structure of the electrode is analyzed, and the last section gives a short summary.

II. MODEL AND THEORETICAL DESCRIPTION

A. Model Hamiltonian

We consider a linear chain of electron sites (QD chain, atomic chain) coupled to one or more electron reservoirs or placed on a substrate. We are going to study time dynamics of the system electronic states after the quench and analyze the spectral density (local DOS) related to all chain sites. We mainly concentrate on the geometry with the electrode coupled via the first site to the chain. The total time-dependent Hamiltonian for this system can be written in the second quantization notation as a sum of two parts: $H(t) = H_0 + V(t)$, where

$$H_0 = \sum_{\alpha} \sum_{k\alpha} \varepsilon_{k\alpha} c_{k\alpha}^{\dagger} c_{k\alpha} + \sum_{i=1}^N \varepsilon_i c_i^{\dagger} c_i \quad (1)$$

stands for a single electron term describing electrons in the leads or in the chain, respectively. The coupling term is responsible for the electron tunneling between the system sites:

$$V(t) = \sum_{i=1}^{N-1} V_{i,i+1}(t) c_i^{\dagger} c_{i+1} + \sum_{i,k\alpha} V_{i,k\alpha}(t) c_{k\alpha}^{\dagger} c_i + \text{H.c.} \quad (2)$$

Here $c_{k\alpha}$ ($c_{k\alpha}^{\dagger}$), c_i (c_i^{\dagger}) are the usual annihilation (creation) operators for an electron in lead α with wave vector k and for an electron at the i th chain site, respectively. The chain is composed of N sites described by single electron states ε_i , $i = 1, \dots, N$, where neighboring sites are coupled via tunnel matrix elements, $V_{i,i+1}(t)$, which in general can be time dependent. The leads are modeled as ideal Fermi gasses with electron energies $\varepsilon_{k\alpha}$, which are coupled to the chain sites via the time-dependent tunnel matrix elements $V_{i,k\alpha}(t)$, and the electron dispersion in all leads is spin independent. With the above Hamiltonian we assume that electron-electron interactions do not lead to correlation effects, like the Kondo effect, and are negligible (for small interactions they can be captured by an effective shift of the on-site energies in the chain). Then both spin directions are independent of each other, such that the spin is not considered explicitly. For some coupled QD systems or for Au or Pb chains on vicinal silicon surfaces, these conditions are met reasonably well.

B. Evolution operator method

We are going to investigate the system dynamics due to the time-dependent perturbation (quantum quench). Time evolution of the local DOS at all chain sites is described in terms of the evolution operator $U(t, t_0)$ and reads [22]

$$\rho_i(E, t) = \sum_{\alpha} D_{\alpha}(E) |U_{i,k\alpha}(t, t_0)|^2, \quad (3)$$

where k vector corresponds to the electron state with energy E , $U_{i,k\alpha}(t, t_0) = \langle i|U|k\alpha\rangle$, and $D_{\alpha}(E)$ is the lead's DOS and the zero temperature case is assumed. The evolution operator elements in the interaction representation can be obtained from the following equation:

$$i \frac{dU(t, t_0)}{dt} = U_0(t, t_0) V(t) U_0^{\dagger}(t, t_0) U(t, t_0), \quad (4)$$

where $U_0(t, t_0)$ describes the evolution of the H_0 term, $U_0(t, t_0) = T \exp(i \int_{t_0}^t H_0 dt')$, and T denotes the time ordering. In the above equation it is assumed that $\hbar = 1$ and for $t < t_0$ all electron states in the system are decoupled, i.e., the couplings are switched on at $t = t_0$, leading to the transient effects in the system for $t > t_0$. From the knowledge of the appropriate evolution operator matrix elements $U(t, t_0)$, one can find the local DOS as well as the electron occupation number at a given site, the transmittance, or the currents flowing in the system [39,40,43–45]. These elements satisfy the following integro-differential Volterra equation of the second kind [obtained from Eq. (4)]:

$$\begin{aligned} \frac{dU_{i,kL}(t)}{dt} &= -iV_{i,i+1} e^{i(\varepsilon_i - \varepsilon_{i+1})t} U_{i+1,kL}(t) \\ &\quad - iV_{i,i-1} e^{i(\varepsilon_i - \varepsilon_{i-1})t} U_{i-1,kL}(t) - i\delta_{i,1} V_{1,kL} e^{i(\varepsilon_i - \varepsilon_{kL})t} \\ &\quad - \delta_{i,1} V_{1,kL}^2 \int_0^t dt' D_L(t-t') e^{i\varepsilon_i(t-t')} U_{i,kL}(t'), \end{aligned} \quad (5)$$

where we assume $t_0 = 0$ [thus $U_{i,kL}(t, t_0) = U_{i,kL}(t)$] and consider only one electron reservoir coupled to the first chain site, $\alpha = L$ (for other configurations the equation has a similar structure). Here, $D_L(t-t') = \int dE D_L(E) \exp[-iE(t-t')]$ is the Fourier transform of the electron density of

states in the electrode. Equation (5) is really the set of complex equations for every i and k , and assuming the chain length $N = 20$ and the number of k vectors in the lead is about 500, we have to solve $20 \times 500 = 10\,000$ differential equations for only one time point t . Note also that the Fourier transforms of the lead DOS, $D(t - t')$, have no analytical form [besides some specific $D(E)$ functions], thus the problem is not trivial and in general analytical solutions of these equations do not exist. The problem can be simplified a bit using a wide-band approximation for the lead, i.e., it is assumed that the spectral density of the wire-lead coupling, $\Gamma(E) = 2\pi \sum_{kL} |V_{1,kL}|^2 \delta(E - \varepsilon_{kL}) = \Gamma$, is energy independent. Within this approximation one can obtain the time integral in Eq. (5) and write the last term in the form $-\delta_{i,1} \frac{\Gamma}{2} U_{1,kL}(t)$.

C. Analytical solutions

In our further studies we consider a regular and symmetrical chain composed of the same kind of sites, i.e., all on-site energies are the same, $\varepsilon_i = \varepsilon_0$, and there is the same coupling strength between the neighboring sites, $V_{i,j} = V$ for $t > 0$. In such a case Eq. (5) takes the form

$$\frac{dU_{i,kL}(t)}{dt} = -iV[U_{i+1,kL}(t) + U_{i-1,kL}(t)]$$

$$F_j(s) = \frac{-V_{j,kL} i^j V^{j-1}}{[s - i(\varepsilon_0 - \varepsilon_{kL})]} \frac{\prod_{j_1=1}^{N-j} (s + 2iV \cos \frac{j_1 \pi}{N-j+1})}{\prod_{j_1=1}^N (s + 2iV \cos \frac{j_1 \pi}{N+1}) + \frac{\Gamma}{2} \prod_{j_1=1}^{N-1} (s + 2iV \cos \frac{j_1 \pi}{N})}, \quad (9)$$

for which the inverse Laplace transformation (i.e., the evolution operator) is hard to obtain due to the sum of s polynomials in the denominator; thus, in general one has to find $U_{i,kL}(t)$ numerically from the coupled set of differential equations, Eq. (6). Note that for some special cases we can derive analytical formulas for the inverse Laplace transform of Eq. (9) and, e.g., assuming $N = 1$, one finds $F_1(s) = \frac{-V_{1,kL}}{[s - i(\varepsilon_0 - \varepsilon_{kL})](s + \frac{\Gamma}{2})}$, and $U_{1,kL}(t) = \frac{-V_{1,kL}}{\varepsilon_0 - \varepsilon_{kL} - i\frac{\Gamma}{2}} (e^{i(\varepsilon_0 - \varepsilon_{kL})t} - e^{-\frac{\Gamma}{2}t})$. Also, for $N = 2$, exact analytical solutions are possible, as in the case $F_i(s) = \frac{-V_{i,kL}(is\delta_{i,1} + \delta_{i,2}V)}{[s - i(\varepsilon_0 - \varepsilon_{kL})](s - \frac{\Gamma}{4} + 2Vx)(s - \frac{\Gamma}{4} - 2Vx)}$, where $i = 1, 2$, $x = \sqrt{(\frac{\Gamma}{4V})^2 - 1}$, and because its denominator is expressed by the product of three terms one can obtain analytically the inverse Laplace transformation for $F_i(s)$. In this case, for $\varepsilon = \varepsilon_0 = 0$ this inverse transformation has a relatively simple form: $U_{1,kL}(t) = \frac{-V_{1,kL}}{Vx} e^{-\frac{\Gamma}{4}t} \sinh(Vxt)$, and similar for $i = 2$. For larger N , one can transform the sum in the denominator of Eq. (9) into the product expression using the following approximation: $\prod_{j_1=1}^N (s + 2iV \cos \frac{j_1 \pi}{N+1}) \simeq (s + 2iV \cos \frac{N\pi}{N+1}) \prod_{j_1=1}^{N-1} (s + 2iV \cos \frac{j_1 \pi}{N})$, which allows us to obtain the inverse transformation for the evolution operator matrix elements in the following analytical form:

$$U_{j,kL}(t) = \frac{-V_{j,kL} V^{j-1} \prod_{j_1=1}^{N-j} (\varepsilon_0 - \varepsilon_{kL} + 2V \cos \frac{j_1 \pi}{N-j+1})}{(\varepsilon_0 - \varepsilon_{kL} - i\frac{\Gamma}{2} + 2V \cos \frac{N\pi}{N+1}) \prod_{j_1=1}^{N-1} (\varepsilon_0 - \varepsilon_{kL} + 2V \cos \frac{j_1 \pi}{N})} e^{i(\varepsilon_0 - \varepsilon_{kL})t} \\ + \frac{V_{j,kL} V^{j-1} \prod_{j_1=1}^{N-j} [i\frac{\Gamma}{2} + 2V (\cos \frac{j_1 \pi}{N-j+1} - \cos \frac{N\pi}{N+1})]}{(\varepsilon_0 - \varepsilon_{kL} - i\frac{\Gamma}{2} + 2V \cos \frac{N\pi}{N+1}) \prod_{j_1=1}^{N-1} [i\frac{\Gamma}{2} + 2V (\cos \frac{j_1 \pi}{N} - \cos \frac{N\pi}{N+1})]} e^{-\frac{\Gamma}{2}t} e^{-2iV \cos \frac{N\pi}{N+1}t} \\ + \sum_{j_1=1}^{N-1} \frac{V_{j,kL} V^{j-1} \prod_{j_2=1}^{N-j} [2V (\cos \frac{j_2 \pi}{N-j+1} - \cos \frac{j_1 \pi}{N})] e^{-2iV \cos \frac{j_1 \pi}{N}t}}{(\varepsilon_0 - \varepsilon_{kL} + 2V \cos \frac{j_1 \pi}{N}) [i\frac{\Gamma}{2} + 2iV (\cos \frac{N\pi}{N+1} - \cos \frac{j_1 \pi}{N+1})] \prod_{j_2=1, j_2 \neq j_1}^{N-1} [2V (\cos \frac{j_2 \pi}{N} - \cos \frac{j_1 \pi}{N+1})]} \quad (10)$$

Note that for the system geometry in which the chain is on the substrate, i.e., all sites are coupled to electron reservoirs,

$$-i\delta_{i,1} \left[V_{1,kL} e^{i(\varepsilon_0 - \varepsilon_{kL})t} - i\frac{\Gamma}{2} U_{i,kL}(t) \right]. \quad (6)$$

To resolve analytically the above set of differential equations we apply the Laplace transformation method, $\mathcal{L}\{U_{j,kL}(t)\} = F_j(s)$, which leads to the following algebraic equations:

$$sF_j(s) = -iV[F_{j-1}(s) + F_{j+1}(s)] \\ - \delta_{j,1} \frac{iV_{j,kL}}{s - i(\varepsilon_0 - \varepsilon_{kL})} - \delta_{j,1} \frac{\Gamma}{2} F_j(s). \quad (7)$$

The solution of this equation can be written in short analytical form,

$$F_j(s) = -V_{j,kL} \frac{i^j V^{j-1} \det A_{N-j}^0}{\det A_N [s - i(\varepsilon_0 - \varepsilon_{kL})]}, \quad (8)$$

where A_N is a tridiagonal matrix (dimension $N \times N$) composed of the following elements: $(A_N)_{ij} = \delta_{i,j} s + \delta_{i,j \pm 1} iV + \delta_{i,1} \delta_{j,1} \frac{\Gamma}{2}$, and A_{N-j}^0 matrix (dimension $N - j \times N - j$) corresponds to A matrix but for $\Gamma = 0$ (system decoupled from the leads). In our case $\det A_N = \det A_N^0 + \frac{\Gamma}{2} \det A_{N-1}^0$. The determinant of a regular tridiagonal matrix, A_N^0 , satisfies the recurrence relation and can be expressed by means of the Chebyshev polynomials of the second kind [46]. Using the product representation for this determinant, for the considered system with the electrode coupled to the first site of the chain, one obtains

as well as for the chain between two leads, the Laplace transformation has a similar structure to Eq. (9), and its inverse

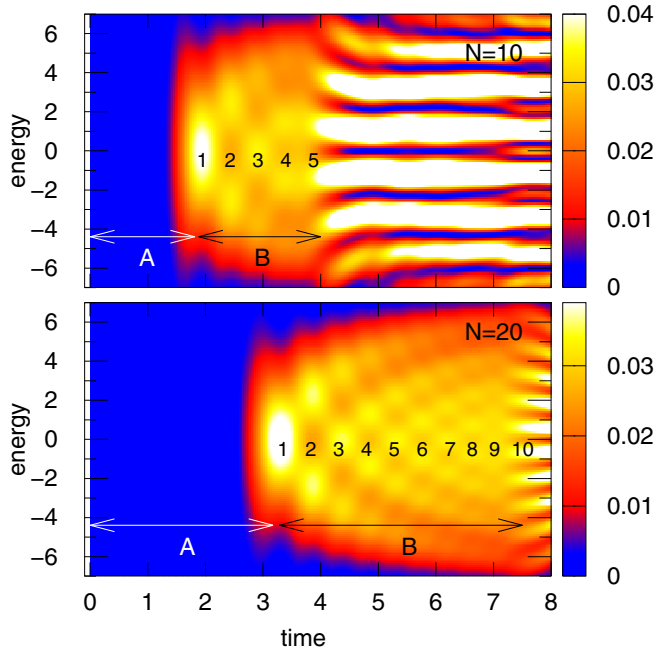


FIG. 1. Spectral density function $\rho_N(E, t)$ of a linear chain composed of $N = 10$ (upper panel) and $N = 20$ sites (bottom panel) after the quench at $t = 0$ (for $t < 0$: $\Gamma = 0$, $V_i = V = 0$ and for $t > 0$: $\Gamma_L = 1$, $V = 4$), $\varepsilon_0 = 0$. A and B indicate the flat density area and the transient crystal region, respectively. The reference energy point is the lead Fermi energy, $E_F = 0$, and energy is expressed in Γ units and time in \hbar/Γ units.

transformation for specific cases leads to exact analytical solutions for $U_{i,kL}(t)$, but they do not have short and transparent forms. In our calculations all energies are expressed in units of $\Gamma_L = \Gamma \equiv 1$ and time in \hbar/Γ units (which for $\Gamma = 1$ meV equals 0.6 ps). Moreover, the energy reference point is the electrode Fermi energy, $E_F = 0$.

III. RESULTS: 1D TRANSIENT CRYSTALS

In the beginning we consider a linear quantum chain suddenly coupled to the left electrode (at time $t = 0$) and concentrate on the transient effects. In Fig. 1 we analyze time dynamics of the spectral density function (local DOS at the last chain site), $\rho_N(E, t)$, for the chain composed of $N = 10$ and $N = 20$ sites, upper and bottom panels, respectively. As one can see, there are a few characteristic areas of the local DOS in time. Most important are regions A and B, indicated in both panels by arrows. The former region is responsible for the signal travel from the lead to the last site of the system just after the quench. Thus, it is characterized by a flat DOS until the signal (information) appears at the end site. The appearance in time of the local DOS peak at this site (for $E = \varepsilon_0 = 0$) depends on the chain length N , and for longer chains the electrode signal needs more time to reach the last site, cf. region A in both panels. The second area, region B, shows a very regular pattern of the local DOS peaks which changes periodically in time; it stands for the transient crystal area. Such a local DOS pattern was observed earlier for the two-site system, where the signal bounced from site to site,

leading to a similar pattern of DOS [22]. However, the nature of the patterns discussed here for a 1D chain of N sites is quite different: first, after some time from the quench, the energy level at the last site of the chain, $i = N$, “sees” the electrode signal and its spectral function forms one peak in DOS (end of region A, $t = 1.95$ in the upper panel). Then the information from the last but one site, $i = N - 1$, reaches the last site, and the spectral density splits and has two peaks for a while, for $t = 2.45$, similar to DOS of the stationary two-site system. Next, the information from the third site from the end, $i = N - 2$, reaches the last site and gives a three-peaked DOS structure at this site for $t = 2.95$, and so on. Thus, the local DOS structure changes in time, and when the last site sees all system sites (end of region B, $t = 4$ in the upper panel), it tends to the equilibrium DOS of the chain characterized by N local peaks. This effect observed in region B is called a 1D transient crystal and is also visible in the bottom panel for $N = 20$ sites.

The black numbers in both panels indicate the effective length of the transient crystal N_{eff} , which is dynamically formed in our 1D system. However, there is something unexpected here: the transient crystal pattern suddenly vanishes for $N_{\text{eff}} = 5$ or $N_{\text{eff}} = 10$ (upper and bottom panels), even the chain is twice as long. This phenomenon is related to the impulse propagation between the chain sites. When the lead impulse travels along the whole chain, the signal from the first sites starts to balance between the neighboring sites and their local DOS changes earlier than the rest sites. And when the last chain site sees the lead, the middle site of the chain receives information about the first half of the sites. So now this information needs only half the chain length to travel towards the last chain site. After that time, all sites in the chain see each other. Thus, the transient crystal pattern is suddenly destroyed (at the end of the B area) and an N -peaked structure of DOS appears. It confirms that the transient structure of the local DOS is not a usual interference pattern of some electron states but it stands for a nonequilibrium physical process in which each chain site interchanges information about its spectral density function with all chain sites.

It was shown that the lead signal after the quench needs some time to reach a given atomic site (it does not appear in the chain immediately). As the impulse spreads along the chain, the local DOS at a given site changes in time. We assume that the signal reaches a chain site i for such time τ_i that the first maximum in the spectral density function $\rho_i(E, t)$ appears. This situation is shown in Fig. 2 (upper panel), where the local DOS at the Fermi level at sites $i = 1$ (solid line) and $i = 20$ (broken line) are depicted as a function of time (here $\tau_1 = 0.45$ and $\tau_{20} = 3.31$ time units). The bottom panel depicts the impulse propagation time through the whole chain τ_i for different chain lengths, $N = 20, 40$, and for the site-site couplings $V = 1, 2, 4$, respectively. The horizontal axis represents the number of sites in the chain ($i = 1, 2, \dots, N$), and the lines are plotted for better visualization. The results indicate that the signal spreads linearly through the chain and the propagation rate does not depend on the chain length N (the curves for $N = 20$ and $N = 40$ overlap). Thus, one expects a constant impulse velocity through the chain in region A. However, the results also show that for weaker and weaker site-site coupling V , (for fixed N) our impulse needs more

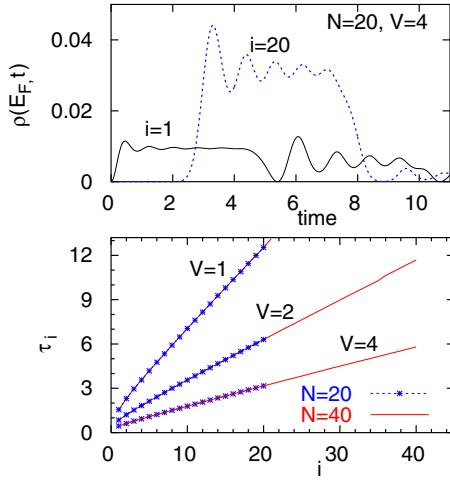


FIG. 2. Time evolution of the spectral density function at the Fermi level for $V = 4$, $N = 20$ at the first and last chain sites, $i = 1$ and $i = 20$ (upper panel)—first maxima at these curves appear for time $\tau_1 = 0.45$ and $\tau_N = 3.31$. The bottom panel shows the time of first maxima in $\rho_i(E, t)$ for every chain site i for $N = 20$ (blue points) and $N = 40$ (red lines) and for different couplings $V = 1, 2$, and 4 . The other parameters are the same as in Fig. 1.

time to reach a given chain site, i.e., the curves for smaller V are steeper. This dependence on V seems to not be linear and will be analyzed in more detail. In Fig. 3 we concentrate on the first and last chain sites and show times τ_1 and τ_N (upper and bottom panel, respectively) as a function of the coupling strength between the sites V . It is interesting that the time of the first local DOS maximum at the first site τ_1 is independent of the chain length N (the curves overlap each other), but it depends on V , although the signal from the electrode flows

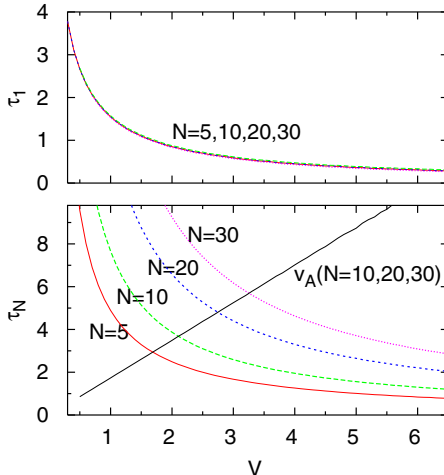


FIG. 3. Time of the first maximum in the spectral density function $\rho_1(E, t)$, i.e., at the first site (τ_1 , upper panel) and $\rho_N(E, t)$ at the last site (τ_N , bottom panel), as a function of the coupling parameter V for $N = 5, 10, 20$, and 30 sites. The black line in the bottom panel corresponds to the velocity of the signal propagation through area A, $v_A = \frac{N}{\tau_N - \tau_1}$, as a function of the site-site coupling V . The values of v_A correspond the same scale as time values on the y axis. The other parameters are the same as in Fig. 1.

directly from the lead to the first site. One can obtain this time for the first maximum in DOS analytically as $\tau_{\max} = \frac{\ln(\frac{V}{V+x})}{Vx}$, and for very large V this time tends to zero (the chain can be treated as a single molecule). It is also the reason that the time propagation to the last chain site τ_N (bottom panel) for large V vanishes. However, in this case τ_N depends on the chain length N (the longer chain the larger propagation time). For very small coupling V the sites are almost separate from each other and the signal hardly reaches the last site, so τ_N increases to infinity. Note also that for thermodynamic limit, i.e., for greater and greater N , one should wait more and more time to observe the transient crystal patterns, and for an infinite chain length there are also an infinite number of DOS states that contribute to smooth local DOS so the transient crystal can hardly be observed in this case.

From the knowledge of the chain length N (which stands for a distance for the lead impulse to cover) and propagation time along the chain τ_N , one can obtain the impulse velocity in region A, v_A , which is also analyzed in the bottom panel in Fig. 3 (solid line). It turns out that it is directly proportional to the coupling strength V . Thus, for small V the velocity decreases (impulse cannot spread in the system), and for larger V the system sites are strongly coupled and it is much easier to propagate such a signal along the chain (the velocity linearly increases). It is worth noting that the impulse velocity in region A does not depend on the chain length N , and the lines for various N almost overlap.

Now we are going to analyze impulse dynamics (its propagation) in the transient crystal time span, i.e., in region B. In Fig. 4 (upper panel) we show the local DOS at the last site of the chain composed of $N = 20$ sites suddenly quenched with the electrode via the first site (which is the same as in Fig. 1). The transient crystal region is easily seen with a changing number of peaks in time. The local DOS structure for a given time reminds the spectral function (DOS) of the stationary 1D crystal of the length N_{eff} ; thus, using the equation of motion for the retarded Green's function, $G^r(E)$ [47], we obtain the stationary DOS for different chain lengths, $\rho_N^0(E) = -\frac{1}{\pi} \text{Im} G_N^r(E)$, and compare them with the time-dependent DOS at the last site. The circles in the upper panel represent the energy positions of peaks in the stationary DOS obtained for the effective chain lengths N_{eff} (white numbers). As one can see, the agreement between the time-dependent structure of the local DOS at the last site and the static 1D chain DOS is quite satisfying.

To analyze further the transient crystal dynamics, we study time positions of the local DOS peaks for different coupling strengths V and adjust them to the stationary chain length N_{eff} . The results are depicted in Fig. 4 (bottom panel) for the site-site couplings $V = 1, 2$, and 4 , and for three chain lengths, $N = 20, 40$, and 60 (as indicated in the legend). Here, Δt stands for a time interval between the first and next peaks in the local DOS (each peak in the time-dependent DOS corresponds to the stationary DOS for the chain length $N_{\text{eff}} = 1, 2, \dots$), so Δt delivers information on how fast the electric signal from the inside sites reaches the last one and how fast the transient crystal structure is formed. It is easily seen that for a given coupling strength V , this dependence is linear, which leads to the regular transient crystal pattern in time. It means that there is a constant impulse speed between the sites,

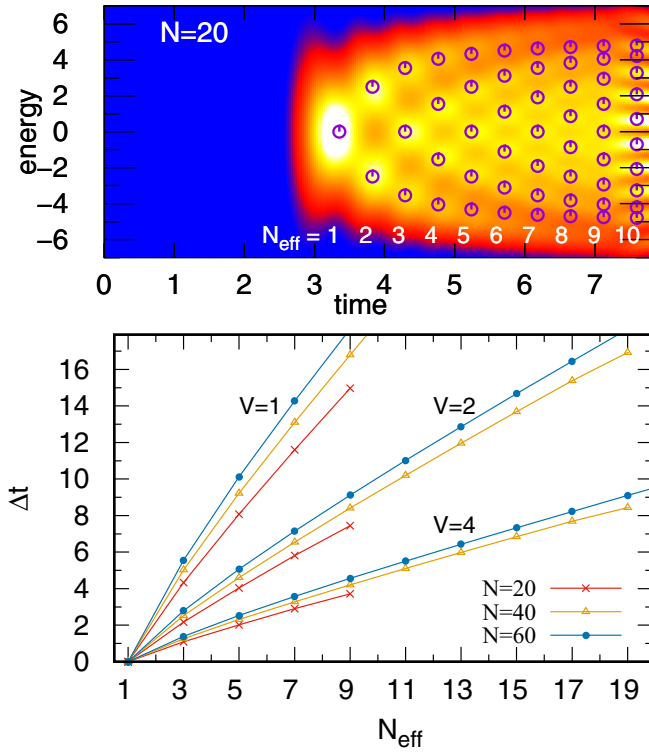


FIG. 4. Time-dependent spectral density function $\rho_N(E, t)$ (upper panel) for $V = 4$ and $N = 20$ with indicated effective chain lengths of the transient crystal N_{eff} from 1–10. The circles correspond to maxima of the stationary DOS obtained for a linear chain composed of the N_{eff} site, and for the effective coupling $V_{\text{eff}} = V/3.2 \cos(\frac{\pi}{N_{\text{eff}}+1})$ and $\varepsilon_i = 0$. The bottom panel shows the time difference between the first and next maxima in $\rho_N(E, t)$ in the transient crystal area as a function of the effective chain length N_{eff} for $N = 20, 40, 60$ (red crosses, orange triangles, and blue circles, respectively) and for $V = 1, 2,$ and 4 (as indicated in the panel). The lines are plotted for better visualization. The other parameters are the same as in Fig. 1.

v_B (obtained as a distance of the effective chain length, N_{eff} , divided by Δt). Note that one can also define a time period for a transient crystal which is inversely proportional to the impulse velocity; however, the pattern of the transient crystal is not strictly periodic, i.e., if for a given time t the local DOS corresponds to a chain of the length N_{eff} , then after the time period one does not observe the same local DOS structure but the structure which corresponds to a $N_{\text{eff}} + 1$ length chain.

For weaker coupling V between sites, the signal propagates much slower in the system (large Δt) and the impulse velocity in area B, v_B , decreases. Of course, the transient crystal pattern is destroyed for $N_{\text{eff}} = \frac{N}{2}$ (as was discussed earlier), so it exists only for a certain period of time after the quench. Note, however, that the impulse propagation time Δt (and thus v_B) depends also on the chain length N , and it increases with increasing N , e.g., for $V = 1$ the fifth maximum in DOS ($N_{\text{eff}} = 5$) appears for $\Delta t = 8.1$ for the chain length $N = 20$ (or $\Delta t = 9.2$ for $N = 40$ and $\Delta t = 10.1$ for $N = 60$). It can be understood that for longer chains there are more peaks in the structure of the local DOS and it is more difficult to rebuild such a structure in time. One can say that there is a

TABLE I. Signal velocity in regions A and B for different chain lengths $N = 20, 40, 60$. The velocity is expressed in units of distance between sites per $\frac{\hbar}{\Gamma}$ (time unit).

| v_A | v_B | v_B | v_B |
|------------------|----------|----------|----------|
| $N = 20, 40, 60$ | $N = 20$ | $N = 40$ | $N = 60$ |
| 1.74 V | 0.67 V | 0.59 V | 0.56 V |

kind of inertia of the local DOS to change themselves in time (for a larger number of peaks this inertia increases). Note that for horizontal geometry (each site is coupled to the surface electrode) Δt is also a linear function of N_{eff} .

To summarize the impulse propagation along the chain, one can notice that in region A the impulse velocity v_A does not depend on the chain length N , but it increases linearly with the site-site coupling V (as shown in Fig. 3, bottom panel). The line coefficient is 1.74 in this case, which is shown in Table I, left column. Also, the impulse velocity in the transient crystal region B, v_B , is a linear function of the coupling V , but more importantly, it depends also on the chain length and slightly decreases with increasing N , right three columns in Table I. It can be explained by the local DOS inertia, which leads to slower impulse propagation in time for larger N . It is also the reason that we have significantly different impulse velocities in regions A and B, i.e., $v_A \simeq 3v_B$. In region A the signal (or information from the lead) travels through atomic states of the chain, so it is much faster than for the impulse propagation through the local DOS with many peaks (in the transient crystal region). One can estimate the impulse speed in a real 1D chain assuming the lattice constant between QDs equals $1 \mu\text{m}$ and $\Gamma = 1 \text{ meV}$, the time unit $\frac{\hbar}{\Gamma}$ equals $6.6 \times 10^{-13} \text{ s}$, one obtains the velocity unit of about $10^6 \frac{\text{m}}{\text{s}}$.

IV. BEYOND THE WIDE-BAND LIMIT

Now, we consider more realistic models of the lead spectral density and check how DOS singularities influence the transient crystal structure in the chain. For an electrode which is characterized by nontrivial band structure with peaks, gaps, or surface states, the wide-band limit approximation fails and one should describe lead electrons in a more adequate way, which is a nontrivial task, especially for time-dependent studies [40–43]. One expects that peaks in the electrode DOS can strengthen the transient pattern and increase the impulse velocity in the system. In our calculations we take into consideration three different DOS structures of the electrode, i.e., flat rectangular DOS (called DOS_A), two-dimensional (2D) tight-binding DOS with a single van Hove peak in the middle of the band (DOS_B), and DOS with two van Hove peaks with a local minimum in the middle of the band (DOS_C), [48,49]—these functions correspond to different 2D atomic lattices. The calculations are performed using a complex set of differential Volterra equations, Eq. (5), and the Fourier transform of the lead DOS (needed in the time integral) is obtained numerically, except the rectangular DOS, where $D(E) = \frac{\Theta(w/2 - |E|)}{w}$ (w is the DOS bandwidth and Θ is the Heaviside step function), for which a simple analytical solution exists, $D(t) = \frac{\sin(tw/2)}{tw/2}$. The results for the chain spectral

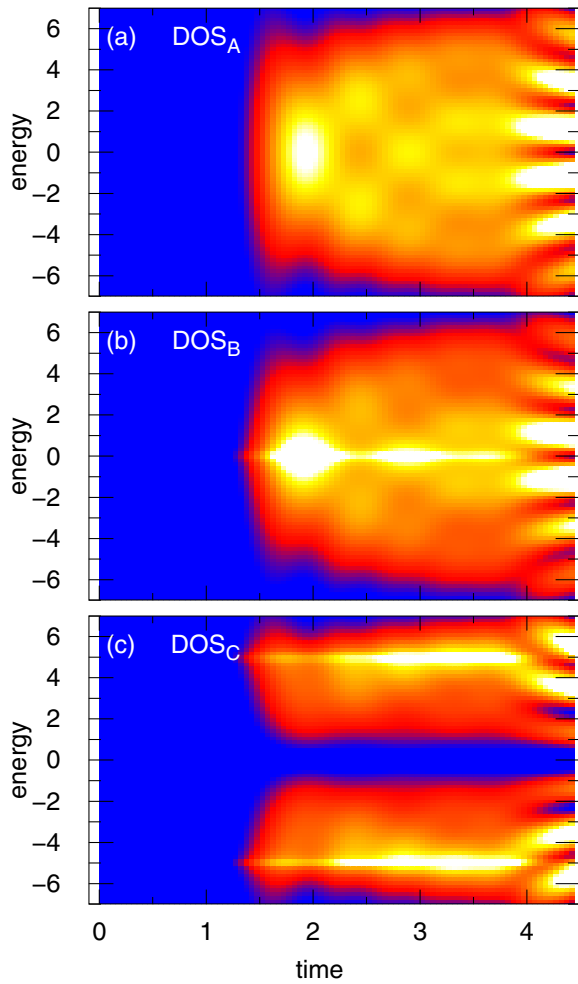


FIG. 5. Time-dependent spectral density function $\rho_N(E, t)$ after the quench at $t = 0$ for chain length $N = 10$ and coupling strength $V = 4$, for different lead DOS: (a) rectangular DOS, (DOS_A), (b) 2D square lattice DOS with one van Hove singularity for $E = 0$ (DOS_B), and (c) 2D honeycomb (hexagonal) lattice DOS with two van Hove singularities for $E = \pm 5$ (DOS_C) [48,49]. All DOS curves have the width $w = 30\Gamma$ and they are all normalized. The other parameters are the same as in Fig. 1.

density at the last chain site, $\rho_N(E, t)$, are shown in Fig. 5 for $N = 10$ sites. The upper panel corresponds to the rectangular DOS of the electrode, and as one can see, the transient crystal structure is almost the same as in Fig. 1 (upper panel for $N = 10$), with local maxima of DOS appearing for the same energies and time. It confirms that for a flat DOS a wide-band approximation can be safely applied. For the lead DOS with the van Hove singularity in the middle of the band, i.e., for $\varepsilon = 0$, DOS_B , panel b, the transient crystal structure around the zero energy is, as expected, clearly strengthened. Thus, the larger the lead DOS value, the larger the local DOS peaks observed in the chain (and the more evident the transient crystal

pattern). However, although the transient crystal structure is easily seen, there is no change in the time and energy positions of the peaks. Thus, the signal velocities v_A and v_B through the chain and in the transient crystal region do not depend on the lead DOS at all. The bottom panel (c) depicts the result for the lead DOS characterized by two van Hove singularities and the local minimum in the middle of the band (for $E = 0$). In this case, the local DOS near the zero energy is strongly suppressed, which leads to a vanishing transient crystal pattern. On the other hand, the local DOS corresponding to the energies of the van Hove peaks (for $E = \pm 5$) is significantly amplified. Therefore, in the presence of a real electrode the transient crystal pattern in the chain can still be observed, assuming there are no energy gaps in the structure of the lead DOS.

V. CONCLUSIONS

The time-dependent transient properties of a linear system composed of N coupled sites (QDs or atoms) were studied using the evolution operator technique and the tight-binding Hamiltonian. We have concentrated on the chain spectral density (local DOS) dynamics and its evolution in time after the quench. Within the Laplace transform technique some analytical formulas for the evolution operator matrix elements were derived which were used to obtain the chain electrical properties. It was found that the electrode signal propagates linearly through the system, depending on the hopping integrals between sites, and the chain spectral density function reveals a very regular structure of peaks which oscillate in time. The energy positions of these peaks for a given time correspond to the stationary DOS positions of the 1D crystal; thus, such a time-dependent structure stands for a phenomena called the transient crystal, which exists in the time domain. However, in comparison with our earlier studies for the two-site system, the transient crystal pattern of a linear chain has a somewhat different origin and suddenly vanishes when the last chain site sees all other sites. Note that for 1D transient crystals the local DOS does not recur in time but changes regularly every time span, so it cannot be strictly classified as a time crystal.

It was also shown that the impulse velocity through the system just after the quench is a few times larger in comparison with the signal propagation in the transient crystal area where the information balances between the neighboring sites. It results from the local DOS inertia, as in the nonequilibrium case it takes much more time to rebuild a many-peaked structure of DOS. Moreover, we have found that the transient crystal pattern in a linear chain can also be observed for real electrodes characterized by the van Hove singularities or by a flat spectral density.

ACKNOWLEDGMENT

This work was partially supported by National Science Centre, Poland, under Grant No. 2018/31/B/ST3/02370.

[1] J. N. Crain, J. L. McChesney, F. Zheng, M. C. Gallagher, P. C. Snijders, M. Bissen, C. Gundelach, S. C. Erwin, and F. J.

Himpfel, Chains of gold atoms with tailored electronic states, *Phys. Rev. B* **69**, 125401 (2004).

- [2] A. Baski, K. Saoud, and K. Jones, 1-D nanostructures grown on the Si(5 5 12) surface, *Appl. Surf. Sci.* **182**, 216 (2001).
- [3] M. Jałochowski, T. Kwapiński, P. Łukasik, P. Nita, and M. Kopciuszynski, Correlation between morphology, electron band structure, and resistivity of Pb atomic chains on the Si(5 5 3)-Au surface, *J. Phys.: Condens. Matter* **28**, 284003 (2016).
- [4] T. H. Oosterkamp, L. P. Kouwenhoven, A. E. A. Koolen, N. C. van der Vaart, and C. J. P. M. Harmans, Photon Sidebands of the Ground State and First Excited State of a Quantum Dot, *Phys. Rev. Lett.* **78**, 1536 (1997).
- [5] W. G. van der Wiel, S. De Franceschi, J. M. Elzerman, T. Fujisawa, S. Tarucha, and L. P. Kouwenhoven, Electron transport through double quantum dots, *Rev. Mod. Phys.* **75**, 1 (2002).
- [6] S. Kohler, J. Lehmann, and P. Hänggi, Driven quantum transport on the nanoscale, *Phys. Rep.* **406**, 379 (2005).
- [7] L. P. Kouwenhoven, A. T. Johnson, N. C. van der Vaart, A. van der Enden, C. J. P. M. Harmans, and C. T. Foxon, Quantized current in a quantum dot turnstile, *Z. Phys. B* **85**, 381 (1991).
- [8] R. H. Blick, R. J. Haug, J. Weis, D. Pfannkuche, K. v. Klitzing, and K. Eberl, Single-electron tunneling through a double quantum dot: The artificial molecule, *Phys. Rev. B* **53**, 7899 (1996).
- [9] S. K. Watson, R. M. Potok, C. M. Marcus, and V. Umansky, Experimental Realization of a Quantum Spin Pump, *Phys. Rev. Lett.* **91**, 258301 (2003).
- [10] G. Platero and R. Aguado, Photon-assisted transport in semiconductor nanostructures, *Phys. Rep.* **395**, 1 (2004).
- [11] L. E. F. Foa Torres, H. L. Calvo, C. G. Rocha, and G. Cuniberti, Enhancing single-parameter quantum charge pumping in carbon-based devices, *Appl. Phys. Lett.* **99**, 092102 (2011).
- [12] T. Fujisawa, D. G. Austing, Y. Tokura, Y. Hirayama, and S. Tarucha, Electrical pulse measurement, inelastic relaxation, and non-equilibrium transport in a quantum dot, *J. Phys.: Condens. Matter* **15**, R1395 (2003).
- [13] F. M. Souza, Spin-dependent ringing and beats in a quantum dot system, *Phys. Rev. B* **76**, 205315 (2007).
- [14] R. Taranko and T. Kwapiński, Charge and current beats in t-shaped qubit-detector systems, *Phys. E* **70**, 217 (2015).
- [15] N. H. Lindner, G. Refael, and V. Galitski, Floquet topological insulator in semiconductor quantum wells, *Nat. Phys.* **7**, 490 (2011).
- [16] G. Usaj, P. M. Perez-Piskunow, L. E. F. Foa Torres, and C. A. Balseiro, Irradiated graphene as a tunable floquet topological insulator, *Phys. Rev. B* **90**, 115423 (2014).
- [17] S. Camalet, J. Lehmann, S. Kohler, and P. Hänggi, Current Noise in ac-Driven Nanoscale Conductors, *Phys. Rev. Lett.* **90**, 210602 (2003).
- [18] S. Camalet, S. Kohler, and P. Hänggi, Shot-noise control in ac-driven nanoscale conductors, *Phys. Rev. B* **70**, 155326 (2004).
- [19] F. Wilczek, Quantum Time Crystals, *Phys. Rev. Lett.* **109**, 160401 (2012).
- [20] K. Sacha, Modeling spontaneous breaking of time-translation symmetry, *Phys. Rev. A* **91**, 033617 (2015).
- [21] K. Sacha and J. Zakrzewski, Time crystals: A review, *Rep. Prog. Phys.* **81**, 016401 (2018).
- [22] M. Kurzyna and T. Kwapiński, Nontrivial dynamics of a two-site system: Transient crystals, *Phys. Rev. B* **102**, 245414 (2020).
- [23] S. Choi, J. Choi, R. Landig, G. Kucsko, H. Zhou, J. Isoya, F. Jelezko, S. Onoda, H. Sumiya, V. Khemani, C. von Keyserlingk, N. Y. Yao, E. Demler, and M. D. Lukin, Observation of discrete time-crystalline order in a disordered dipolar many-body system, *Nature (London)* **543**, 221 (2017).
- [24] J. Zhang, P. W. Hess, A. Kyprianidis, P. Becker, A. Lee, J. Smith, G. Pagano, I.-D. Potirniche, A. C. Potter, A. Vishwanath, N. Y. Yao, and C. Monroe, Observation of a discrete time crystal, *Nature (London)* **543**, 217 (2017).
- [25] B. Buča, J. Tindall, and D. Jaksch, Non-stationary coherent quantum many-body dynamics through dissipation, *Nat. Commun.* **10**, 1730 (2019).
- [26] F. Iemini, A. Russomanno, J. Keeling, M. Schirò, M. Dalmonte, and R. Fazio, Boundary Time Crystals, *Phys. Rev. Lett.* **121**, 035301 (2018).
- [27] P. Kongkhambut, J. Skulte, L. Mathey, J. G. Cosme, A. Hemmerich, and H. Keßler, Observation of a continuous time crystal, *Science* **377**, 670 (2022).
- [28] A. Kshetrimayum, J. Eisert, and D. M. Kennes, Stark time crystals: Symmetry breaking in space and time, *Phys. Rev. B* **102**, 195116 (2020).
- [29] T. M. Gunawardana and B. Buča, Dynamical 1-bits and persistent oscillations in stark many-body localization, *Phys. Rev. B* **106**, L161111 (2022).
- [30] A. Cabot, F. Carollo, and I. Lesanovsky, Metastable discrete time-crystal resonances in a dissipative central spin system, *Phys. Rev. B* **106**, 134311 (2022).
- [31] F. Machado, D. V. Else, G. D. Kahanamoku-Meyer, C. Nayak, and N. Y. Yao, Long-Range Prethermal Phases of Nonequilibrium Matter, *Phys. Rev. X* **10**, 011043 (2020).
- [32] E. Barnes, J. M. Nichol, and S. E. Economou, Stabilization and manipulation of multispin states in quantum-dot time crystals with Heisenberg interactions, *Phys. Rev. B* **99**, 035311 (2019).
- [33] S. Sarkar and Y. Dubi, Signatures of discrete time-crystallinity in transport through an open fermionic chain, *Commun. Phys.* **5**, 155 (2022).
- [34] S. Sarkar and Y. Dubi, Emergence and dynamical stability of a charge time-crystal in a current-carrying quantum dot simulator, *Nano Lett.* **22**, 4445 (2022).
- [35] R. Taranko, T. Kwapiński, and T. Domański, Transient dynamics of a quantum dot embedded between two superconducting leads and a metallic reservoir, *Phys. Rev. B* **99**, 165419 (2019).
- [36] E. Taranko, M. Wiertel, and R. Taranko, Transient electron transport properties of multiple quantum dots systems, *J. Appl. Phys.* **111**, 023711 (2012).
- [37] T. Kwapiński and R. Taranko, Charging time effects and transient current beats in horizontal and vertical quantum dot systems, *Phys. E* **63**, 241 (2014).
- [38] A.-P. Jauho, N. S. Wingreen, and Y. Meir, Time-dependent transport in interacting and noninteracting resonant-tunneling systems, *Phys. Rev. B* **50**, 5528 (1994).
- [39] R. Taranko, T. Kwapiński, and E. Taranko, Influence of microwave fields on electron transport through a quantum dot in the presence of direct tunneling between leads, *Phys. Rev. B* **69**, 165306 (2004).
- [40] Y.-Q. Zhou, R.-Q. Wang, L. Sheng, B. Wang, and D. Y. Xing, Pumped spin and charge currents from applying a microwave

- field to a quantum dot between two magnetic leads, *Phys. Rev. B* **78**, 155327 (2008).
- [41] J. Maciejko, J. Wang, and H. Guo, Time-dependent quantum transport far from equilibrium: An exact nonlinear response theory, *Phys. Rev. B* **74**, 085324 (2006).
- [42] Y. Zhu, J. Maciejko, T. Ji, H. Guo, and J. Wang, Time-dependent quantum transport: Direct analysis in the time domain, *Phys. Rev. B* **71**, 075317 (2005).
- [43] T. Kwapiński, R. Taranko, and E. Taranko, Band structure effects in time-dependent electron transport through the quantum dot, *Phys. Rev. B* **66**, 035315 (2002).
- [44] T. Kwapiński and R. Taranko, Time-dependent transport through a quantum dot with the over-dot (bridge) additional tunneling channel, *Phys. E* **18**, 402 (2003).
- [45] T. Grimley, V. Jyothi Bhasu, and K. Sebastian, Electron transfer in the reflection of atoms from metal surfaces, *Surf. Sci.* **124**, 305 (1983).
- [46] T. Kwapiński, Charge fluctuations in a perfect and disturbed quantum wire, *J. Phys.: Condens. Matter* **18**, 7313 (2006).
- [47] T. Kwapiński, Conductance oscillations of a metallic quantum wire, *J. Phys.: Condens. Matter* **17**, 5849 (2005).
- [48] T. C. Choy, Density of States for a Two-Dimensional Penrose Lattice: Evidence of a Strong Van-Hove Singularity, *Phys. Rev. Lett.* **55**, 2915 (1985).
- [49] T. Horiguchi, Lattice Green's functions for the triangular and honeycomb lattices, *J. Math. Phys.* **13**, 1411 (1972).